IEEE Access
Multidisciplinary | Rapid Review | Open Access Journal

Received August 2, 2019, accepted September 25, 2019, date of publication October 2, 2019, date of current version October 17, 2019.

Digital Object Identifier 10.1109/ACCESS.2019.2945245

Symphotic Design of an Edge Detector for Autonomous Navigation

ROBERTO ZECCA, DANIEL L. MARKS, AND DAVID R. SMITH, (Member, IEEE)
Center for Metamaterials and Integrated Plasmonics, Department of Electrical and Computer Engineering, Duke University, Durham, NC 27708, USA
Corresponding author: Roberto Zecca (roberto.zecca@duke.edu)

This work was supported by the Air Force Office of Scientific Research (AFOSR) under Grant FA9550-18-1-0187.

ABSTRACT Autonomous navigation systems rely on the collection and processing of large datasets with advanced and memory-intensive algorithms. The requirements in terms of computing power and energy consumption can be significant. In this work, we propose a passive electromagnetic structure that can reduce the computational load by detecting edges (obstacles) in the far field. This is accomplished by probing the scene and processing its scattering on the physical layer, at the speed of light in the medium. By using a recently developed inverse design method, we present an edge detector able to detect obstacles at 15 different locations with an average efficiency of 97% and minimal crosstalk. We call this class of devices that can integrate a vast number of distinct optical functions with high efficiency *symphotic*.

INDEX TERMS Autonomous automobiles, electromagnetic metamaterials, inverse problems.

I. INTRODUCTION

The last decade has seen an enormous amount of interest and resources devoted to autonomous vehicles. In particular, the public and the scientific community have concentrated on autonomous ground vehicles, which have been undergoing on-road testing in the last three years, and UAVs (umanned aerial vehicles, or drones). While there are varying degrees of automation that these vehicles can attain [1] (ranging from relatively commonplace driver assistance, to conditional automation with driver oversight, all the way to full automation, where a driver is not involved), all autonomous vehicles require additional instrumentation to gather the necessary information to replace a human driver, partially or completely. In particular, higher levels of automation require the vehicle to construct an internal model of its surroundings in order to navigate them successfully and safely. This goal, in general, cannot be attained with any one single technology, but typically requires the synergy of multiple sensing mechanisms [2]. Sensing technologies that are widely used in autonomous vehicles include, for example, odometry, inertial measurements, GPS, sonar, radar, and lidar [3].

Many of the sensing technologies deployed on autonomous vehicles collect large amounts of data, which are then post-processed on board with algorithms such as simultaneous localization and mapping (SLAM) [4], [5] and deep neural networks for autonomous decision-making [6]. While these approaches have showed viable results, they are computationally intensive and power-hungry, often requiring the computing power of graphics processing units (GPUs). To alleviate the computational and energetic load, it may be useful to introduce systems that cheaply pre-process the collected data or that assist the main detection systems in collecting a smaller amount of significant data, e.g., by flagging potentially relevant features in the environment for the main sensors to concentrate on.

In this work, we propose an edge detector based on a recent design method for artificial electromagnetic media [7]. The design method yields designs for complex electromagnetic media that we call "symphotic" materials. These devices are able to simultaneously perform multiple operations (multiplexing) at extremely high efficiencies. In particular, the symphotic edge detector design presented in this work operates by remotely detecting the presence of geometrical edges, which can be markers for obstacles or road hazards, as depicted conceptually in Fig. 1. We demonstrate a symphotic edge-detection design that can scatter 30 incident beams to 30 other scattered beams (15 angles of detection) with efficiencies exceeding 95% and low crosstalk between the beams. In this context, the term "crosstalk" refers to the unwanted

The associate editor coordinating the review of this manuscript and approving it for publication was Ildiko Peter.

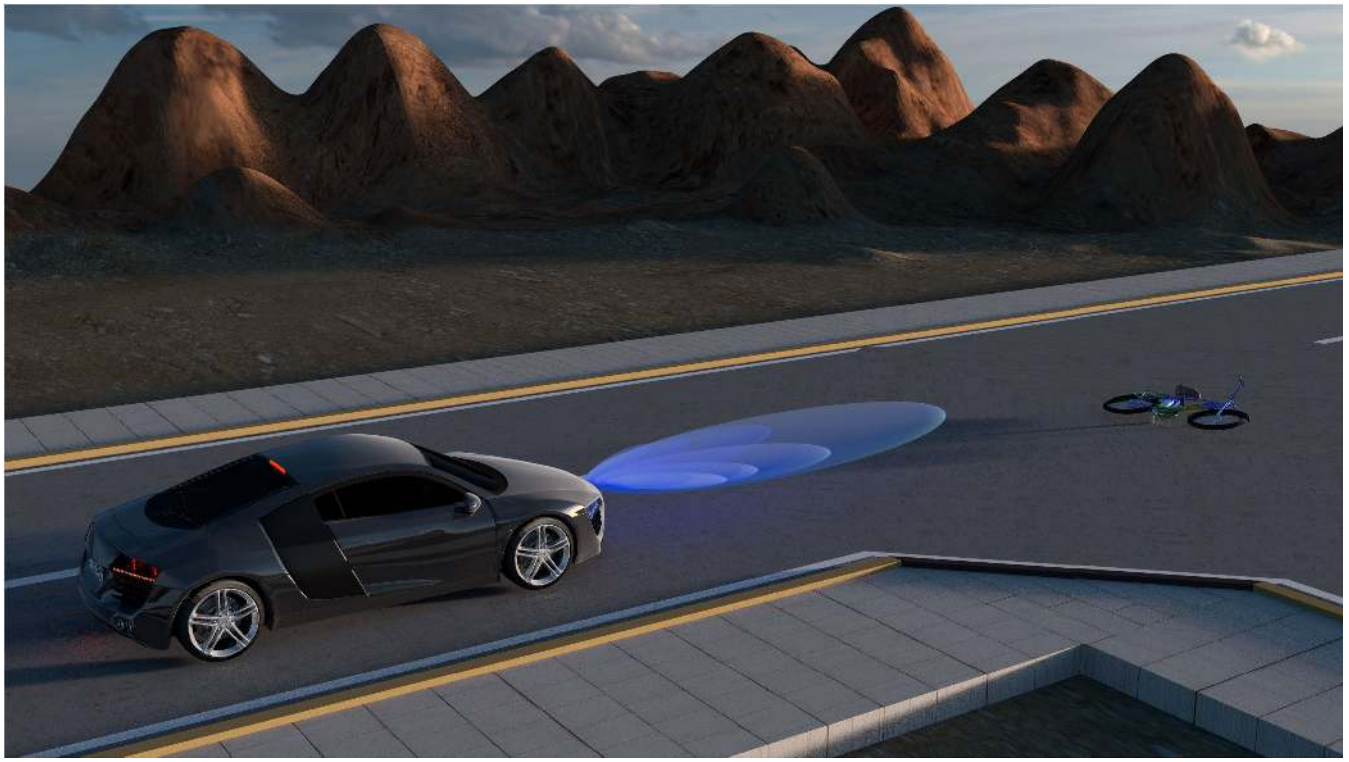

FIGURE 1. Representation of a symphotic edge detector deployed on a car. The device is mounted on the front and it detects the presence of obstacles ahead on the road.

scattering of energy from an input beam into a different output beam than was intended in the design process. As opposed to a camera- or lidar-based detection system, a symphotic edge detector performs the computation on its physical layer, at the speed of light in the medium. This reduces the need for large post-processing power dramatically, with a vast potential for increasing detection speed and reducing cost, complexity, and space/weight requirements.

This article is structured as follows. In Sec. II, we briefly describe the mechanism of edge detection we encode in the symphotic devices. In Sec. III, we summarize the symphotic design method, as it appeared in [7]. In Sec. IV, we describe the architecture of the symphotic edge detector and provide further details on the design specifications and on the practical implementation of the design algorithm. In Sec. V we present the computed results, including the designed properties of several edge detectors, their efficiencies, and other performance metrics. Finally, in Sec. VI we draw conclusions and outline further avenues of research on the topic.

II. PRINCIPLE OF EDGE DETECTION

From their inception, radars have been used to track targets. Initially, a target was tracked by pointing the antenna so as to maintain the maximum scattered power from the target. As the target moves, however, the captured power decreases; thus, the antenna must seek the direction to which the target moved in order to restore the backscattered power. If multiple feedpoints are placed at the focus of a radar [8] reflector dish, the feedpoints may be fed with signals of opposite phase. When a target crosses between the beams formed by each of the feedpoints, the target scatters back a signal such that the sign of the return phase indicates the direction of travel of the target. This return is a simple error signal that may be used, for example, by a servo mechanism to keep the antenna pointed at the target. By directly generating beams that encode the state of the target motion as radar returns, the interpretation of the data is made much simpler, and the system is able to respond more quickly to a rapidly changing environment, because a great deal of additional measurement and computation is avoided.

The benefit of symphotic materials is that, among other uses, they may be designed to project many structured beams into the environment and capture scattered signals matching other structured beams, without compromising efficiency significantly as more beams are added. Therefore, unlike the tracking radars, which mechanically or otherwise sequentially point to targets, many targets may be simultaneously illuminated. The target's movement is not required for the symphotic edge detector to work, but in a realistic setting there would usually be relative movement between vehicle and target.

In our symphotic realization, each target point is tracked by two designed beams, one of which projects a pattern onto the target, and a second that detects the signal scattered from the target. As schematized in Fig. 2, the pattern projected on the target is a zeroth order Gauss-Hermite beam. A target

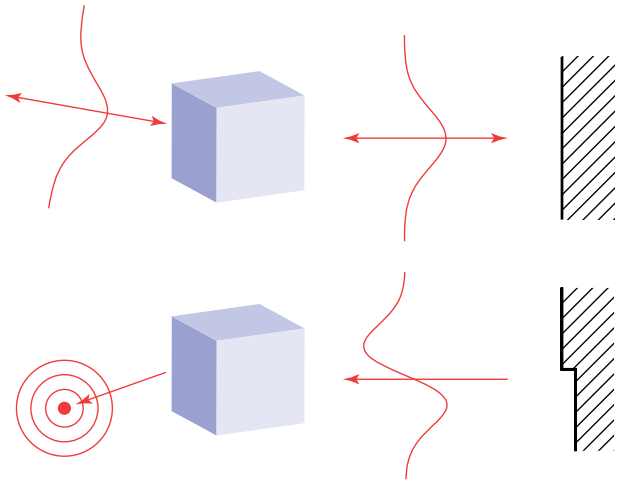

FIGURE 2. Principle of edge detection with a symphotic device. (top) The device redirects a fundamental Gaussian radiation source to probe in a given direction. If the beam reflects off a flat surface, its wavefront is not altered significantly and the beam feeds back into the source. (bottom) If the beam reflects off an edge, the reflected wave changes shape to a Gaussian of first order, which has a node in its center. The symphotic edge detector collects this different wave and concentrates it onto a sensor.

that is uniformly scattering over the beam reflects it back with a phase shift. Therefore, by reciprocity, the scattered power feeds back into the source that was used to synthesize the probing beam. A target that has an edge centered on the probing beam will scatter the zeroth-order Gauss-Hermite beam into a superposition of Gauss-Hermite modes, with a strong first-order Gauss-Hermite component. This first-order Gauss-Hermite beam is the second pattern encoded in the edge detector, which reroutes it onto a detector. The two opposite-phase lobes of the first-order beam serve the same purpose as the two feedpoints of the radar reflector antenna.

Therefore, this arrangement can be used to detect when an edge moves into the beams as an increased signal is detected. For applications such as autonomous vehicles, this may be used to locate road curbs, obstructions, or other obstacles and threats. As the signal processing required is minimal, the navigation system may respond quickly to the situation.

In order to design a radar system to simultaneously monitor and detect scatterers from multiple directions, one must simultaneously project these beams and collect the backscattered radiation. For millimeter-wave radiation, each beam would require a more traditional two-dimensional aperture on the order of hundreds of square centimeters, and therefore an infeasible area would be required to accommodate all these apertures if they were separated at the grille of an automobile. Instead, a single three-dimensional structure that shares a single aperture (entry face) for all the beams may be designed that simultaneously projects the zeroth-order beams onto the target and collects the scattered radiation with the first-order beams. Using the specification of the pairs of incident and scattered beams, the symphotic design method determines a single distribution of polarizable elements that efficiently scatters each incident beam to its respective scattered beam. Each ideal point dipole may be practically realized, for example, by using a subwavelength dielectric structure with the same polarizability.

III. SYMPHOTIC DESIGN METHOD

When considering electromagnetic devices, one often defines the operation of those devices in terms of the rays or waves that enter and exit it. For example, the imaging operation of a lens may be specified as transforming plane waves to focused points. Rarely, however, is one able to use a specification of these incident and scattered fields to find the medium of a device that achieves the desired operation. This is the inverse scattering problem and is in general difficult to solve. In particular, finding a single material that can—for example with efficiencies approaching 100%—scatter several incident waves to their respective scattered waves is especially difficult, with few general solutions known. The symphotic method [7], which combines the coupled-dipole formalism and a variational formulation of the inverse scattering problem, has proved an efficient way to simultaneously solve multiple inverse scattering problems. "Symphotic" means "light together" (from the Greek *syn-* "together" and *phos* "light") because of the large number of electromagnetic devices that may be simultaneously incorporated into a single volume using this method.

The symphotic method is an inverse design method for metamaterial-based devices and has demonstrated its ability to generate high-efficiency multiplex devices. Compared to more traditional methods such as holography, our technique allows the designed media to exhibit stronger, non-perturbative scattering, which opens the way to a wider solution space, where innovative designs may be found. In [7], however, the highest multiplex number (the number of input-output waves encoded in the device) was three. The method shows promise for much higher multiplex numbers, but massive multiplexing devices have not yet been demonstrated with this method, in neither computation nor experiment. In this work, we explore the capabilities of the design method by designing high-multiplexing devices that are able to encode tens of different input-output wave transformations with high efficiency and low crosstalk.

The remainder of this section briefly summarizes the symphotic design method. The method relies on three elements: the coupled-dipole model (CDM, a modeling technique particularly well-suited for metamaterials and artificial media [9]–[15]), the variational principle, and the adjoint-state method. These three techniques, combined, allow us to tackle the inverse scattering problem as follows: using the adjoint-state method, it is possible to re-formulate the problem of transforming N input waves into desired output waves by splitting it into $2N$ sub-problems (primal and adjoint), all sharing the same medium. By the variational principle, there exists a functional F at whose stationary points the $2N$ sub-problems, together with the properties of the medium, satisfy Maxwell's equations [7], [16], [17]. In the symphotic method, we find the variation of F with respect to the properties of the

medium; we implement an iterative algorithm that alternates updates of the medium to updates of the fields in the sub-problems. The CDM equation is a particularly convenient forward model (equation to solve to obtain the fields) in the context of artificial media, such as metamaterials and symphotic devices, because it reduces the complexity of a continuously varying homogenized medium to a collection of electromagnetic point dipoles, thus reducing Maxwell's equations from differential to algebraic. The CDM also has very attractive computational properties, as it scales in manageable way with the number of electromagnetic dipoles in the problem [18].

The CDM states the Lippman-Schwinger equation for electromagnetic point dipoles. For the case of electric dipoles, to which we limit ourselves in this work, it reads

$$\sum_{j=1}^{N} M_{ij} E_j = E_{\mathrm{inc},i} \quad \forall i \in [1, N_d], \text{ with} \tag{1}$$

$$M_{ij} \equiv \delta_{ij} - G_{ij}\alpha_j, \tag{2}$$

where E is the total field and E_{inc} is the incident field in the absence of a medium, N_d is the total number of dipoles, δ_{ij} is Kronecker's delta, α_j is the polarizability of the j-th dipole, and G is the Green's function $G_{ij} \equiv G\left(r_i, r_j\right)$ of the medium when $\alpha_j = 0\ \forall j$ (r_i is the position in real space of the i-th dipole). Polarizability relates dipole moment p and total electric field at the dipole location:

$$p_i \equiv \alpha_i E_i. \tag{3}$$

The polarizability used in this definition is known as *intrinsic* [7], [19]. It requires care in defining Green's function at the origin ($i = j$): its singular real part can be ignored or reduced to a resonance frequency shift [10], [19], whereas its imaginary part accounts for radiation reaction and must be included [10], [11]. The only requirement the following places on the Green's function is the property of reciprocity [7].

Using the adjoint-state theory, the symphotic design method solves the CDM equation separately for each incident and outgoing field (these are specified as time-reversed "incident fields") for a given set of polarizabilities. Splitting the problem thus, the variables solved for are primal total electric fields E and their adjoints E^a. By the electromagnetic variational principle, it can be shown that the solution(s) to the design problem are to be found at the stationary points of the functional

$$F \equiv \sum_{n=1}^{N_w} w_n \left(\langle E_n^a, \hat{L} E_n \rangle - \langle E_{n,\mathrm{inc}}^a, E_n \rangle - \langle E_n^a, E_{n,\mathrm{inc}} \rangle \right), \tag{4}$$

where $\hat{L} = G^{-1}\hat{M}$, N_w is the multiplexing number (number of input-output wave couples) and w_n are optional weighting factors. Solution points in the generalized phase space spanned by α and all E, E^a will have the property $E^* = E^a$ [7], [17]. In this work, we assume α values are temporally nondispersive. The design process, then, consists of alternating the solutions of (1) with updates to polarizability values. The latter can be found by computing how the functional F varies with respect to the variation of α [7] and using a simple gradient-descent update:

$$\alpha^{(p+1)} = \alpha^{(p)} - \gamma\, \nabla_\alpha F^{(p)}, \tag{5}$$

where γ is a small step size and with

$$\nabla_\alpha F = -\sum_{n=1}^{N_w} w_n E_n^{a*} \circ E_n, \tag{6}$$

where $\circ$ is the element-wise (Hadamard) product. The efficiency of each of the N_w encoded transformations can be measured by [7]

$$\eta_n \equiv \frac{j\langle E_n^a, E_n \rangle}{\sqrt{\langle E_n, E_n \rangle \langle E_n^a, E_n^a \rangle}}. \tag{7}$$

Similarly, crosstalk between transformation n and transformation m (with $n \neq m$) may be quantified as

$$\eta_{nm} \equiv \frac{j\langle E_m^a, E_n \rangle}{\sqrt{\langle E_n, E_n \rangle \langle E_m^a, E_m^a \rangle}}, \tag{8}$$

with the understanding that the definition of Eq. (7) is equivalent to η_{nn}.

IV. DESIGN SPECIFICATIONS FOR SYMPHOTIC EDGE DETECTORS

We design symphotic edge detectors, based on the principles outlined in Sec. II. The symphotic devices are constructed out of electric point dipoles. For the sake of clarity of presentation and economy of computation, we present a scalar 2D version of the problem, in which the edge detectors are 2D in the x–y plane and electric fields and point dipoles are oriented out of plane, along $\hat{z}$. The device architecture is presented in Fig. 3: the edge detector collects zeroth-order Gaussian beams in the angular interval $\Delta\varphi_f$ and redirects them to probe a scene in the angular interval $\Delta\varphi_p$. To represent the scattering due to an edge, first-order Gaussian beams impinging in the same angular range $\Delta\varphi_p$ are transformed into zeroth-order Gaussian beams that exit the device in the angular range $\Delta\varphi_d$, where in practice they would be focused onto specialized detectors. Each angular range is divided into $N_w/2$ directions for multiplexing.

We demonstrate four versions of symphotic edge detector, building up in complexity by increasing the number of directions probed for edges $N_w/2$. This requires progressively larger devices, although we want to emphasize that these symphotic devices achieve remarkable efficiency while remaining relatively small optically (linear dimensions of a few tens of wavelengths). All devices consist of a square array of electric dipoles, spaced $\lambda/7$, enveloped in a square shape. The dimensions of each designed device, together with the total number of dipoles, are reported in Table 1. The lower and upper limits $\{\alpha_{\min}, \alpha_{\max}\}$ of the range of allowed polarizabilities correspond, in an infinite medium made of identical polarizable elements, to effective electric susceptibilities of $\{0.08, 1.98\}$ [7], [20], [21].

TABLE 1. Parameters and efficiencies for designed symphotic edge detectors.

# det. angles	Multiplex #	Dimensions	# dipoles	w_0/λ	$\langle\eta\rangle$ (%)	st. dev. (η) (%)
3	6	$15\lambda \times 15\lambda$	11025	4	99.45	0.05
5	10	$20\lambda \times 20\lambda$	19600	4	99.18	0.17
10	20	$20\lambda \times 20\lambda$	19600	5	98.43	0.55
15	30	$35\lambda \times 35\lambda$	60025	9	97.07	0.63

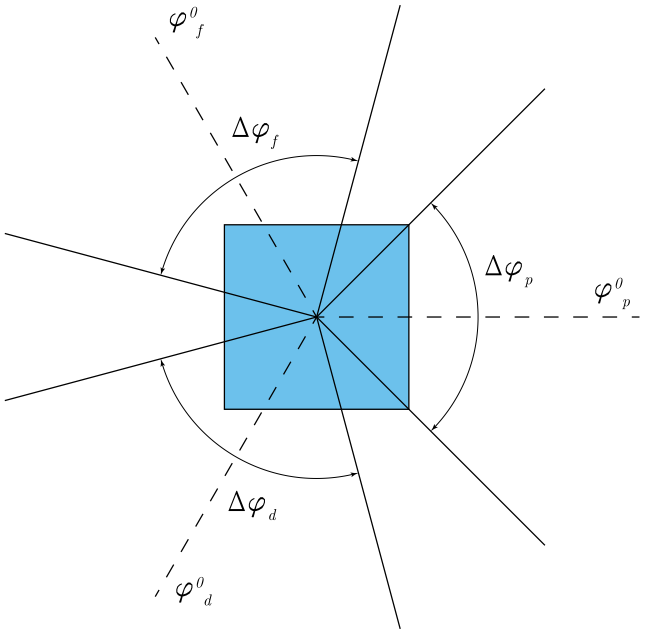

FIGURE 3. Architecture of symphotic edge detector. The device is represented by the square blue box. The first kind of operation consists of Gauss-Hermite zeroth-order "feed" waves, impinging from the angular range $\Delta\varphi_f$, that are redirected into the range $\Delta\varphi_p$ to probe for edges. In the second kind of operation, probed edges reflect Gauss-Hermite first-order waves in the same range $\Delta\varphi_p$; these waves are converted to Gauss-Hermite zeroth-order "detect" waves and focused onto detectors in the range $\Delta\varphi_d$. Each angular range is centered about a central angle φ^0. In this work, $\varphi^0_f = 2\pi/3$, $\varphi^0_p = 0$, and $\varphi^0_d = 4\pi/3$; moreover, $\Delta\varphi_f = \Delta\varphi_p = \Delta\varphi_d = \pi/2$.

The incident and outgoing beams are defined as Gauss-Hermite modes [22], labeled by a single index, since we operate in a 2D geometry. Letting x_l be the coordinate along which the beam propagates and x_t the one perpendicular to it, the modes are

$$\begin{aligned}&\mathrm{GH}_n(x_l, x_t)\\ &= \left(\frac{2}{\pi}\right)^4 \left\{\frac{\exp\left[-j\,(2n+1)\,\psi\,(x_l)\right]}{2^n n! w\,(x_l)}\right\}^{1/2} \times \mathcal{H}_n\left[\sqrt{2}x_t/w(x_l)\right]\\ &\quad \exp\left\{-j\frac{kx_t^2}{2R\,(x_l)} - jkx_l - \left[\frac{x_t}{w\,(x_l)}\right]^2\right\},\end{aligned} \tag{9}$$

where

$$\psi\,(x) \equiv \tan^{-1}\,(x/x_R) \tag{10a}$$

$$x_R \equiv w_0^2 k/2 \tag{10b}$$

$$w\,(x) \equiv w_0\sqrt{1+(x/x_R)^2} \tag{10c}$$

$$\frac{1}{R\,(x)} \equiv \frac{x}{x^2+x_R^2} \tag{10d}$$

and where $\mathcal{H}_n$ is the n-th order Hermite polynomial (physicist convention). The values of w_0 for each designed symphotic edge detector are reported in Table 1.

We evaluate the orthogonality of input and output waves by computing the eigenvalues of their Gram matrix $\bar{\bar{\mathcal{G}}}$ [23] (not to be confused with the matrix form of Green's function $\bar{\bar{G}}$)

$$\mathcal{G}_{ij} \equiv \langle E_i | E_j \rangle. \tag{11}$$

The waves are perfectly orthogonal if all eigenvalues of $\bar{\bar{\mathcal{G}}}$ are equal to one. We choose to tolerate a moderate amount of deviation from this value, understanding that this places a limit on efficiency (upper limit) and crosstalk (lower limit).

The CDM equations are solved using a preconditioned form of the bi-conjugate gradient stabilized method (BiCGSTAB) [24]. Leveraging the placement of dipoles on a regular grid, we implement fast-Fourier-transform (FFT) acceleration [18], which speeds up calculations considerably [7], [18]. In order to better avoid local minima in the functional, we introduce a stochastic aspect to the design cycle, solving for a randomly picked set of $N_w/2$ field couples (both E and E^a) at each iteration and using this partial information to update polarizabilities. We also include a small annealing factor to the gradient-descent step γ to help convergence. Furthermore, we make use of parallel coding techniques and implement the code in MATLAB on a machine with 128 GB of RAM, mounting 12 Intel Core i7-5930K @ 3.50 GHz processors and four NVIDIA GeForce GTX 1080/PCIe/SSE2 graphics-processing units. This makes it possible to design high-N_w devices comprised of several tens of thousands of dipoles in reliably less than three hours.

V. RESULTS

We design symphotic edge detectors for $N = 3$, 5, 10, and 15 angles of detection (corresponding to 6, 10, 20, and 30 multiplexing numbers $N_w = 2N$). The average and standard deviations of efficiencies are reported in Table 1. The polarizabilities of each design are depicted in Fig. 4.

Examples of electric field maps and radiation patterns for each device are depicted in Fig. 5, 6, 7, and 8.[1]

Having measured the efficiency of each encoded function in the edge detectors, we further test the devices by evaluating their ability to correctly identify the presence and position of an edge in their far field. To this end, we follow this procedure:

[1]This paper has supplementary downloadable material, available at http://ieeexplore.ieee.org/. The material includes animated versions of these figures, displaying all functions of each device, as well as values for the individual efficiency for each function of each device.

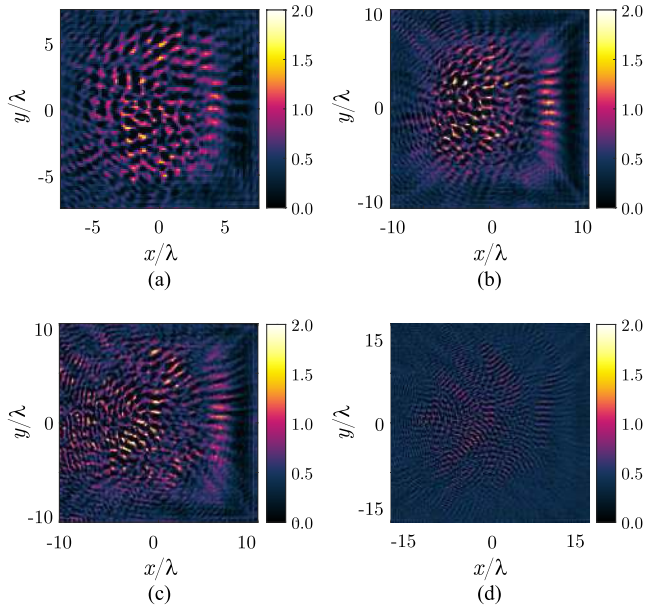

FIGURE 4. Designed edge detectors for (a) 3, (b) 5, (c) 10, and (d) 15 angles of detection. Each panel shows the values of polarizability α as a function of spatial position in the device. The values of polarizability are scaled $\alpha/\epsilon_0 \Delta A$ to units of susceptibility (dimensionless).

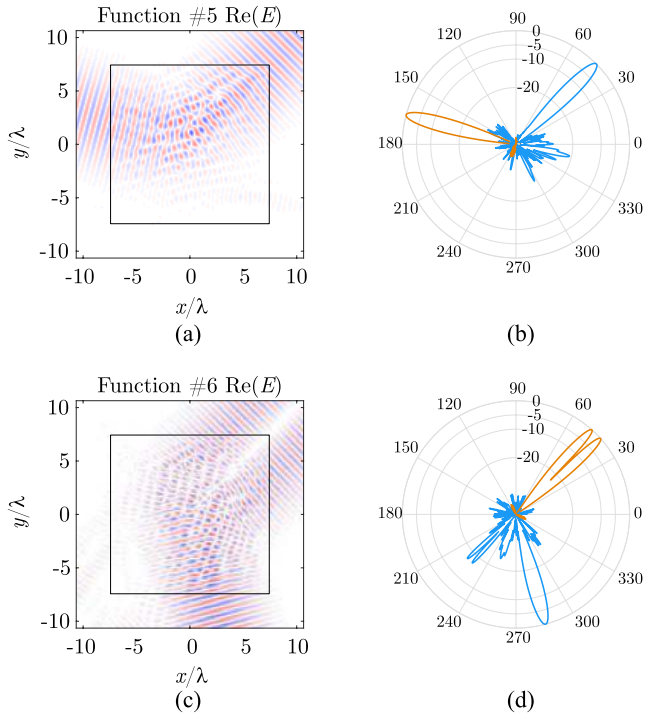

FIGURE 5. Example of electric fields (a,c) and radiation patterns (b,d) for $N = 3$ symphotic edge detector. The top row (a,b) represents a feed-probe function, whereas the bottom row (c,d) represents an edge-detect function. In electric field plots, the square black outline corresponds to the device boundary. In the radiation patterns, the orange lines represent fields that are incident on the device, whereas the blue lines represent fields that are outgoing from the device. Each line is normalized to 0 dB.

1) Select one of the N probing directions φ_j in the range $\Delta\varphi_p$;
2) Place an edge in the far field at φ_j. The edge is modeled as a reflective boundary with reflection coefficient

$$R(\varphi) = \text{sign}\left[\sin\left(\varphi - \varphi_j\right)\right]. \tag{12}$$

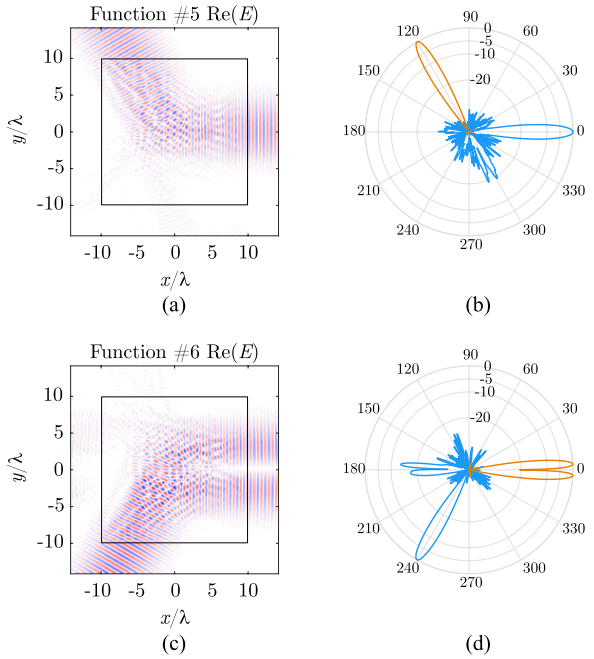

FIGURE 6. Example of electric fields (a,c) and radiation patterns (b,d) for $N = 5$ symphotic edge detector. The top row (a,b) represents a feed-probe function, whereas the bottom row (c,d) represents an edge-detect function. In electric field plots, the square black outline corresponds to the device boundary. In the radiation patterns, the orange lines represent fields that are incident on the device, whereas the blue lines represent fields that are outgoing from the device. Each line is normalized to 0 dB.

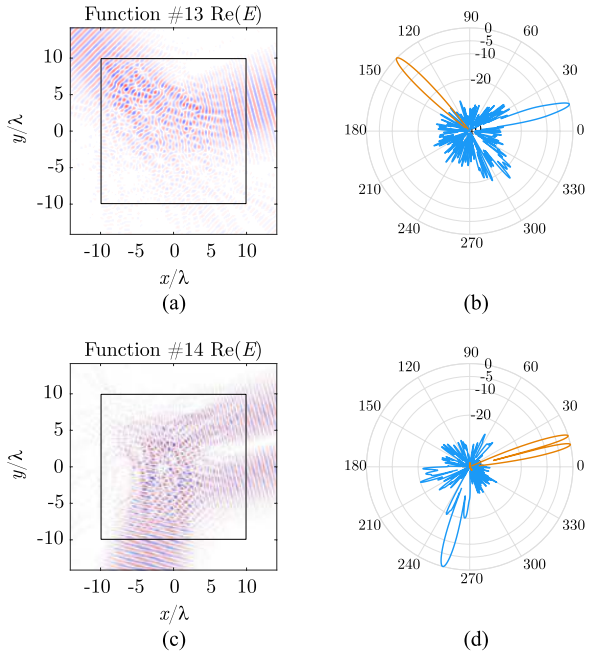

FIGURE 7. Example of electric fields (a,c) and radiation patterns (b,d) for $N = 10$ symphotic edge detector. The top row (a,b) represents a feed-probe function, whereas the bottom row (c,d) represents an edge-detect function. In electric field plots, the square black outline corresponds to the device boundary. In the radiation patterns, the orange lines represent fields that are incident on the device, whereas the blue lines represent fields that are outgoing from the device. Each line is normalized to 0 dB.

3) Select one of the probing waves (outgoing GH_0 beams), propagate it to the far field, and compute the field reflected at the edge;

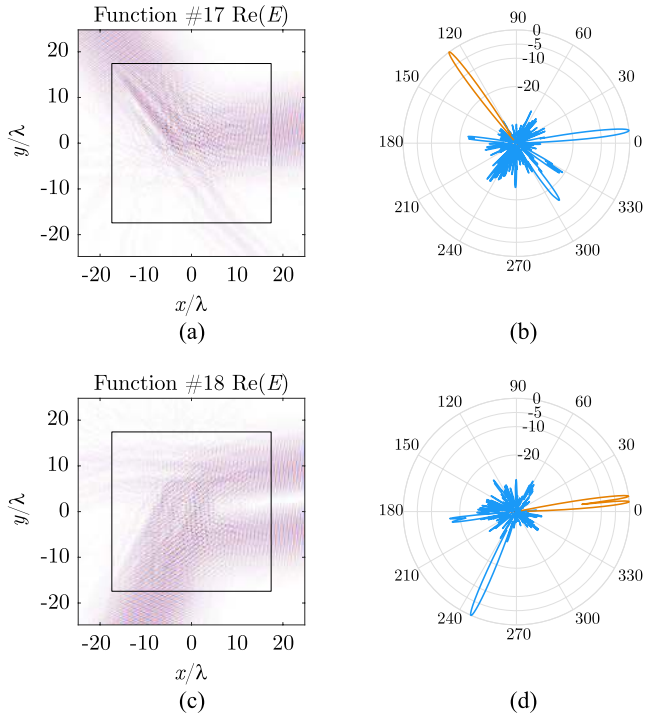

FIGURE 8. Example of electric fields (a,c) and radiation patterns (b,d) for $N = 15$ symphotic edge detector. The top row (a,b) represents a feed-probe function, whereas the bottom row (c,d) represents an edge-detect function. In electric field plots, the square black outline corresponds to the device boundary. In the radiation patterns, the orange lines represent fields that are incident on the device, whereas the blue lines represent fields that are outgoing from the device. Each line is normalized to 0 dB.

4) Propagate the reflected field back to the positions of the dipoles comprising the edge detector. The field reflected by the edge will be a mix of Gauss-Hermite modes, with a relatively strong GH_1 component;
5) Solve the CDM equation for the field reflected by the edge;
6) Project the resulting total field E_t onto each of the N "detect" output waves (in the range $\Delta\varphi_d$), obtaining the total power reaching each detector as

$$\left| \frac{\langle E_k^a, E_t \rangle}{\sqrt{\langle E_k^a, E_k^a \rangle}} \right| \quad \forall k \in [1, N]\,. \tag{13}$$

7) Repeat the procedure for every combination of edge location, probing wave, and detect wave, storing the results in the elements B_{ijk} of a matrix $\bar{\bar{B}}$, where the indices i,j, and k enumerate the probing wave, the edge position, and the detect wave, respectively.

Matrix $\bar{\bar{B}}$ captures all the relevant quantities in the process of testing the performance of a symphotic edge detector. The element B_{ijk} is proportional to the power received by the k-th detector, when an edge at the j-th position is illuminated by the i-th probe wave. Matrix $\bar{\bar{B}}$ has dimensions $N \times N \times N$, and as such it is a fairly large dataset to examine. In order to isolate the positive identification capabilities of an edge detector, subsets of $\bar{\bar{B}}$ can be extracted as two types of "confusion matrices," $\bar{\bar{B}}_1$ and $\bar{\bar{B}}_2$, defined as

$$(B_1)_{ij} \equiv B_{iij} \tag{14a}$$
$$(B_2)_{ij} \equiv B_{ijj}, \tag{14b}$$

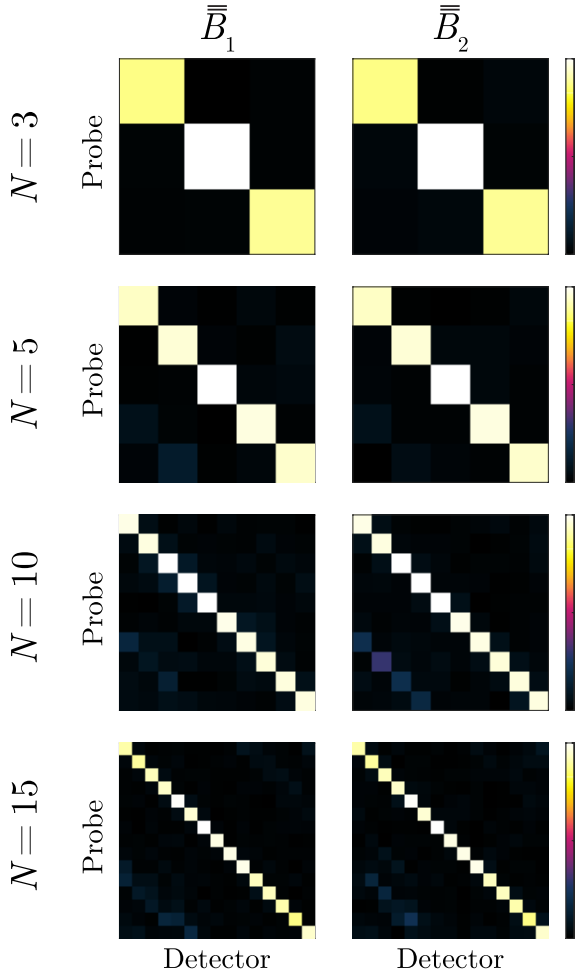

FIGURE 9. Confusion matrices for designed symphotic edge detectors. The matrix entries are plotted on the same color scale device-wise (for each row of panels).

where no Einstein summation convention is implied. Fig. 9 reports the two matrices for each designed symphotic edge detector. Each row of $\bar{\bar{B}}_1$ measures how reliably the "detect" function correctly identifies the position of an edge in the case where the edge is illuminated by its corresponding probe beam, i.e., the one pointing directly at the location of the edge. Each row of $\bar{\bar{B}}_2$, conversely, measures the power scattered by an edge to its corresponding detector, i.e., whether the power at the detector really originated from the beam pointed at the edge or not. The results of Fig. 9 suggest unambiguous performance in the designed edge detectors. A more fully engineered device, which resolves power measurements into binary detection hypotheses, may also employ a form of signal thresholding, which would further reduce the probability of faulty readings.

In Fig. 10, we further show that the symphotic edge detector is able to enact multiple edge-detecting operations at the

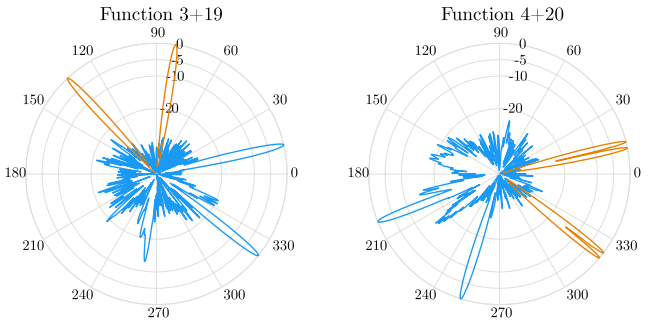

FIGURE 10. Test of $N = 15$ symphotic edge detector enacting two edge-detecting operations concurrently. (left) probing of two angles; (right) detection of the corresponding edges. The radiation patterns are summed incoherently.

same time. In the figure, individual radiation patterns are combined incoherently.

As the results in this section show, the symphotic design method makes it possible to design passive dielectric structures that can multiplex a large number of waves at extremely high efficiencies. Furthermore, as highlighted by Fig. 9, the designed symphotic edge detectors are not only efficient in each of the implemented functions, but are also able to give unambiguous results in the detection of edge positions. Such results would not be possible using more traditional methods such as volume holography, in which large multiplexing numbers come at the expense of significant crosstalk [25]–[27].

VI. CONCLUSION

A symphotic device that projects and receives signals to combine fifteen distinct edge detectors has been designed and simulated. All these operations are performed by the same structure with minimal crosstalk and an average efficiency of 97%. The design method can simultaneously solve for the medium and the thirty fields that satisfy the boundary conditions that generate the beams. To our knowledge, no other inverse-scattering design process can find a solution that combines disparate operations with this efficiency; hence, these devices truly achieve their goal of ''light together.'' The symphotic method transcends the limitations of simplified designs based on ray optics or weak scattering, enabling new types of devices to be realized. This method is not limited to the design of edge detectors for autonomous vehicles. It seems particularly suited to the design of devices able to implement a vast array of linear transformations on the physical layer [28], [29], such as convolutions and other operations that otherwise may require large computational resources on processors or GPUs.

The designs presented in this work are quasi-planar, which makes them amenable to fabrication by addictive manufacturing/3D printing (for longer wavelengths) or by lithographic patterning techniques (for shorter wavelengths). Our research group has obtained excellent results for devices at RF frequencies with 3D printing, which will be presented in a forthcoming work. Three-dimensional symphotic devices, while potentially more versatile and efficient, may pose more of a manufacturing challenge, especially at shorter wavelengths. We suggest that multilayer lithographic fabrication may be a feasible strategy to begin exploring this territory.

ACKNOWLEDGMENT

R. Z. thanks Dr. Nathan Kundtz for his valuable feedback during the preparation of this work.

REFERENCES

[1] *Taxonomy and Definitions for Terms Related to Driving Automation Systems for On-Road Motor Vehicles*, SAE International Standard J3016, 2016.
[2] G. A. Demetriou, ''A survey of sensors for localization of unmanned ground vehicles (UGVs),'' in *Proc. IC-AI*, 2006, pp. 659–668.
[3] G. G. Goyer and R. Watson, ''The laser and its application to meteorology,'' *Bull. Amer. Meteorol. Soc.*, vol. 44, no. 9, pp. 564–570, 1963.
[4] H. Durrant-Whyte and T. Bailey, ''Simultaneous localization and mapping: Part I,'' *IEEE Robot. Autom. Mag.*, vol. 13, no. 2, pp. 99–110, Jun. 2006.
[5] T. Bailey and H. Durrant-Whyte, ''Simultaneous localization and mapping (SLAM): Part II,'' *IEEE Robot. Autom. Mag.*, vol. 13, no. 3, pp. 108–117, Sep. 2006.
[6] B. Huval, T. Wang, S. Tandon, J. Kiske, W. Song, J. Pazhayampallil, M. Andriluka, P. Rajpurkar, T. Migimatsu, R. Cheng-Yue, F. Mujica, A. Coates, and A. Y. Ng, ''An empirical evaluation of deep learning on highway driving,'' 2015, *arXiv:1504.01716*. [Online]. Available: https://arxiv.org/abs/1504.01716
[7] R. Zecca, D. L. Marks, and D. R. Smith, ''Variational design method for dipole-based volumetric artificial media,'' *Opt. Express*, vol. 27, no. 5, pp. 6512–6527, 2019.
[8] M. I. Skolnik, *Radar Handbook*. New York, NY, USA: McGraw-Hill, 1990, ch. 9, pp. 9.1–9.50.
[9] E. M. Purcell and C. R. Pennypacker, ''Scattering and absorption of light by nonspherical dielectric grains,'' *Astrophys. J.*, vol. 186, pp. 705–714, Dec. 1973.
[10] J. E. Sipe and J. van Kranendonk, ''Macroscopic electromagnetic theory of resonant dielectrics,'' *Phys. Rev. A, Gen. Phys.*, vol. 9, no. 5, p. 1806, 1974.
[11] J. Van Kranendonk and J. E. Sipe, ''Foundations of the macroscopic electromagnetic theory of dielectric media,'' in *Progress in Optics*, vol. 15. Amsterdam, The Netherlands: Elsevier, 1977, pp. 245–350.
[12] B. T. Draine, ''The discrete-dipole approximation and its application to interstellar graphite grains,'' *Astrophys. J.*, vol. 333, pp. 848–872, Oct. 1988.
[13] A. Lakhtakia, ''General theory of the Purcell-Pennypacker scattering approach and its extension to bianisotropic scatterers,'' *Astrophys. J.*, vol. 394, pp. 494–499, Aug. 1992.
[14] B. T. Draine and P. J. Flatau, ''Discrete-dipole approximation for scattering calculations,'' *J. Opt. Soc. Amer. A, Opt. Image Sci.*, vol. 11, no. 4, pp. 1491–1499, 1994.
[15] P. T. Bowen, T. Driscoll, N. B. Kundtz, and D. R. Smith, ''Using a discrete dipole approximation to predict complete scattering of complicated metamaterials,'' *New J. Phys.*, vol. 14, no. 3, p. 033038, 2012.
[16] C. H. Chen and C.-D. Lien, ''The variational principle for non-self-adjoint electromagnetic problems,'' *IEEE Trans. Microw. Theory Techn.*, vol. 28, no. 8, pp. 878–886, Aug. 1980.
[17] D. L. Marks and D. R. Smith, ''Inverse scattering with a non self-adjoint variational formulation,'' *Opt. Express*, vol. 26, no. 6, pp. 7655–7671, 2018.
[18] J. J. Goodman, B. T. Draine, and P. J. Flatau, ''Application of fast-Fourier-transform techniques to the discrete-dipole approximation,'' *Opt. Lett.*, vol. 16, no. 15, pp. 1198–1200, 1991.
[19] P. T. Bowen, ''Metamaterials analysis, modeling, and design in the point dipole approximation,'' Ph.D. dissertation, Dept. Elect. Comput. Eng., Duke Univ., Durham, U.K., Jul. 2017.
[20] J. Venermo and A. Sihvola, ''Dielectric polarizability of circular cylinder,'' *J. Electrostat.*, vol. 63, no. 2, pp. 101–117, 2005.
[21] L. D. Landau, J. S. Bell, M. J. Kearsley, L. P. Pitaevskii, E. M. Lifshitz, and J. B. Sykes, *Electrodynamics of Continuous Media* (Course of Theoretical Physics S), vol. 8. Oxford, U.K.: Pergamon Press, 1984, ch. 8, pp. 39–40.
[22] A. E. Siegman, *Lasers*. Sausalito, CA, USA: University Science Books, 1986, ch. 16, pp. 637–646.

[23] D. L. Marks and D. R. Smith, "Mode diversity of weakly modulated cavity antennas," *J. Opt. Soc. Amer. A, Opt. Image Sci.*, vol. 35, no. 1, pp. 135–147, 2018.
[24] H. A. van der Vorst, "Bi-CGSTAB: A fast and smoothly converging variant of Bi-CG for the solution of nonsymmetric linear systems," *SIAM J. Sci. Stat. Comput.*, vol. 13, no. 2, pp. 631–644, 1992.
[25] K. Bløtekjaer, "Limitations on holographic storage capacity of photochromic and photorefractive media," *Appl. Opt.*, vol. 18, no. 1, pp. 57–67, 1979.
[26] D. Brady and D. Psaltis, "Control of volume holograms," *J. Opt. Soc. Amer. A, Opt. Image Sci.*, vol. 9, no. 7, pp. 1167–1182, 1992.
[27] D. Brady and D. Psaltis, "Information capacity of 3-D holographic data storage," *Opt. Quantum Electron.*, vol. 25, no. 9, pp. S597–S610, 1993.
[28] A. Silva, F. Monticone, G. Castaldi, V. Galdi, A. Alù, and N. Engheta, "Performing mathematical operations with metamaterials," *Science*, vol. 343, no. 6167, pp. 160–163, 2014.
[29] N. M. Estakhri, B. Edwards, and N. Engheta, "Inverse-designed metastructures that solve equations," *Science*, vol. 363, no. 6433, pp. 1333–1338, Mar. 2019.

ROBERTO ZECCA was born in Verona, Italy, in 1988. He received the B.S. degree in industrial engineering and the M.S. degree in materials engineering from the University of Trento, Italy, in 2010 and 2013, respectively. He is currently pursuing the Ph.D. degree in electrical and computer engineering with Duke University, under the supervision of Dr. D. R. Smith. His thesis work concentrates mainly on inverse design techniques for volumetric artificial media and metamaterials. As a member of the Smith Research Group, he also researched nonlinear optical processes in nanometric systems, such as lasing in plasmonic nanopatch antennas and the enhancement stimulated Brillouin scattering in waveguides at the nanoscale. He has published four research articles and is an author on two patent applications. His research interests comprise computational electromagnetics and elastomechanics, variational design methods, numerical optimization, holography, and nonlinear optics.

DANIEL L. MARKS was born in Chicago, IL, USA, in 1973. He received the B.S., M.S., and Ph.D. degrees from the University of Illinois at Urbana-Champaign, in 1995, 1998, and 2001, respectively, where he was a Research Scientist with the Biophotonics Laboratory, from 2001 to 2008. In 2009, he joined Duke University, where he is currently an Associate Research Professor with the Department of Electrical and Computer Engineering. He is the author of 85 research articles and holds 17 patents. His research interests include optics, optical design, computational imaging, millimeter-wave and terahertz imaging, metamaterials, and synthetic electromagnetic structures. He has been an Editor of *Applied Optics*.

DAVID R. SMITH (M'03) received the B.S. and Ph.D. degrees in physics from the University of California at San Diego, San Diego, CA, USA, in 1988 and 1994, respectively.

He is currently the James B. Duke Professor of electrical and computer engineering with Duke University and the Director of the Center for Metamaterials and Integrated Plasmonics, Durham, NC, USA. He is also an Adjunct Professor with the Physics Department, University of California at San Diego, an Affiliate Faculty Member with the Electrical and Computer Engineering Department, University of Washington, Seattle, WA, USA, and a Visiting Professor of physics with Imperial College, London, U.K. His research interests include the theory, simulation, and characterization of unique electromagnetic structures, including photonic crystals and metamaterials, as well as applications of such materials.